Article

Kinetic Analysis of Arsenic#Metalation of Human Metallothionein: Significance of the Two-Domain Structure

Thanh T. Ngu, Alexandria Easton, and Martin J. Stillman

J. Am. Chem. Soc., **2008**, 130 (50), 17016-17028 • DOI: 10.1021/ja8060326 • Publication Date (Web): 19 November 2008

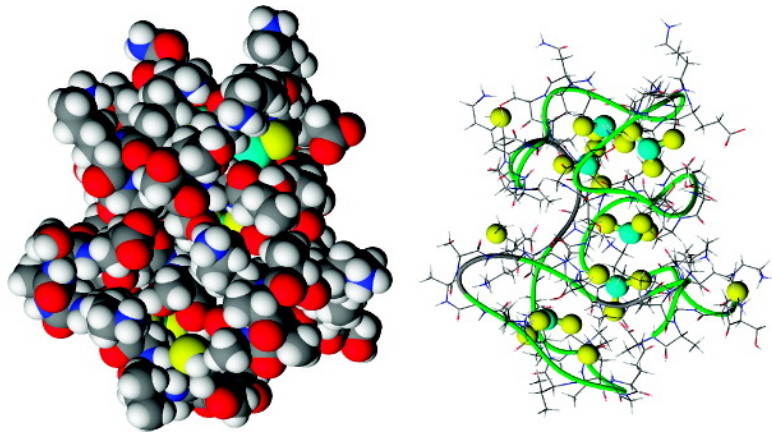

J|A|C|S
ARTICLES

Published on Web 11/19/2008

Kinetic Analysis of Arsenic−Metalation of Human Metallothionein: Significance of the Two-Domain Structure

Thanh T. Ngu, Alexandria Easton, and Martin J. Stillman*

Department of Chemistry, The University of Western Ontario, London, Ontario, Canada, N6A 5B7

Received July 31, 2008; E-mail: Martin.Stillman@uwo.ca

Abstract: Metallothionein (MT) is ubiquitous in Nature, underlying MT's importance in the cellular chemistry of metals. Mammalian MT consists of two metal-binding domains while microorganisms like cyanobacteria consist of a single metal-binding domain MT. The evolution of a two-domain protein has been speculated on for some time; however, no conclusive evidence explaining the evolutionary necessity of the two-domain structure has been reported. The results presented in this report provide the complete kinetic analysis and subsequent mechanism of the As^{3+}-metalation of the two-domain $\beta\alpha$hMT and the isolated single domain fragments using time- and temperature-resolved electrospray ionization mass spectrometry. The mechanism for $\beta\alpha$hMT binding As^{3+} is noncooperative and involves six sequential bimolecular reactions in which the α domain binds As^{3+} first followed by the β domain. At room temperature (295 K) and pH 3.5, the sequential individual rate constants, k_n ($n = 1-6$) for the As^{3+}-metalation of $\beta\alpha$hMT starting at $k_{1\beta\alpha}$ are 25, 24, 19, 14, 8.7, and 3.7 $M^{-1}s^{-1}$. The six rate constants follow an almost linear trend directly dependent on the number of unoccupied sites for the incoming metal. Analysis of the temperature-dependent kinetic electrospray ionization mass spectra data allowed determination of the activation energy for the formation of As_1-H_{17}-$\beta\alpha$hMT (14 kJ mol^{-1}) and As_{2-6}-$\beta\alpha$hMT (22 kJ mol^{-1}). On the basis of the increased rate of metalation for the two-domain protein when compared with the isolated single-domain, we propose that there is an evolutionary advantage for the two-domain MT structures in higher organism, which allows MT to bind metals faster and, therefore, be a more efficient metal scavenger.

Introduction

Metalated and demetalated metallothioneins (MT)[1−8] have been documented since 1957 when Vallee and Margoshes first described horse kidney MT.[9] Mammalian MT consists of 20 cysteines structured into two domains, often described as dumbbell-shaped from the NMR and X-ray structures.[2−5,10,11] A 3-metal, 9-cysteine β cluster and a 4-metal, 11-cysteine α cluster form following metalation with the divalent Group 12 metals Zn^{2+} and Cd^{2+}. The significance of the two domains in MT has long been discussed with frequent suggestions invoking the differential selectivity for metalation of the two domains. For example, it has been reported that the β domain preferentially binds Cu^+ while the α domain preferentially binds Zn^{2+} under these conditions and that each cluster forms independently of constraints or influences from the other cluster.[12−15] However, another study noted that while the two domains assembled independently, the cumulative properties of each domain were not sufficient to describe MT structurally or functionally.[13] Yet studies of the evolutionary distant sea urchin MT have shown a conservation of the two-domain structure, supporting previous conclusions regarding the functional importance of this structural motif.[16,17] We report in this paper new kinetic data that may account for the evolution of a two-domain protein in higher life-forms rather than the single-domain proteins that are observed in lower life-forms like cyanobacteria,[6] *E. fetida*,[18,19]

(1) Ngu, T. T.; Stillman, M. J. *J. Am. Chem. Soc.* **2006**, *128*, 12473–12483.
(2) Kagi, J. H. R.; Nordberg, M. *Metallothionein*, 1st ed.; Birkhauser: Boston, 1978; Vol. 1.
(3) Kagi, J. H. R.; Kojima, Y. *Metallothionein II*, 1st ed.; Birkhauser: Boston, 1985; Vol. 2.
(4) Stillman, M. J.; Shaw, C. F., III.; Suzuki, K. T. *Metallothioneins*, 1st ed.; VCH Publishers: New York, 1992.
(5) Suzuki, K. T.; Imura, N.; Kimura, M. *Metallothionein III*, 1st ed.; Birkhauser: Boston, 1993; Vol. 3.
(6) Blindauer, C. A.; Polfer, N. C.; Keiper, S. E.; Harrison, M. D.; Robinson, N. J.; Langridge-Smith, P. R. R.; Sadler, P. J. *J. Am. Chem. Soc.* **2003**, *125*, 3226–3227.
(7) Krezel, A.; Maret, W. *J. Am. Chem. Soc.* **2007**, *192*, 10911–10921.
(8) Dabrio, M.; Van Vyncht, G.; Bordin, G.; Rodriguez, A. R. *Anal. Chim. Acta* **2001**, *435*, 319–330.
(9) Margoshes, M.; Vallee, B. L. *J. Am. Chem. Soc.* **1957**, 79.
(10) Wehrli, S.; Engeseth, H. R.; Otvos, J. D. *Biochemistry* **1985**, *24*, 6735–6740.
(11) Otvos, J. D.; Armitage, I. M. *Proc. Natl. Acad. Sci. U.S.A.* **1980**, *77*, 7094–7098.
(12) Nielson, K. B.; Winge, D. R. *J. Biol. Chem.* **1984**, *259*, 4941–4946.
(13) Jiang, L.-J.; Vasak, M.; Vallee, B. L.; Maret, W. *Proc. Natl. Acad. Sci. U.S.A.* **2000**, *97*, 2503–2508.
(14) Nielson, K. B.; Winge, D. R. *J. Biol. Chem.* **1985**, *260*, 8698–8701.
(15) Li, H.; Otvos, J. D. *J. Inorg. Biochem.* **1998**, *70*, 187–194.
(16) Riek, R.; Precheur, B.; Wang, Y.; Mackay, E. A.; Wider, G.; Guntert, P.; Liu, A.; Kagi, J. H. R.; Wuthrich, K. *J. Mol. Biol.* **1999**, *291*, 417–428.
(17) Vasak, M.; Hasler, D. W. H. *Curr. Opin. Chem. Biol.* **2000**, *4*, 177–183.
(18) Gehrig, P. M.; You, C.; Dallinger, R.; Gruber, C.; Brouwer, M.; Kagi, J. H. R.; Hunziker, P. E. *Protein Sci.* **2000**, *9*, 395–402.
(19) Gruber, C.; Sturzenbaum, S. R.; Gehrig, P. M.; Sack, R.; Hunziker, P. E.; Berger, B.; Dallinger, R. *Eur. J. Biochem.* **2000**, *267*, 573–582.

10.1021/ja8060326 CCC: $40.75

and funga.[20−22] These single-domain proteins have been shown to contain a highly conserved central segment that correlate to the domain center of mammalian MT and may be considered the core upon which many MTs have evolved.[23]

Metal homeostasis, which is necessary for survival of all organisms, requires buffering of metals via both metalation reactions that store the metals and metal exchange reactions into apoproteins. One of MT's suggested functions involves metal homeostasis; MT appears to play a role in zinc homeostasis as the Zn^{2+} buffering capacity of MT may control cellular Zn availability.[24] This buffering capacity of MT is based on MT's ability to undergo metalation, demetalation and metal exchange reactions. The steady state metalation/demetalation equilibria for MTs are well-known for a large number of metals[7,15,25−28] and numerous metal exchange studies with MT have been documented.[6,13,29,30] While metal exchange in MT has been studied extensively, the detailed mechanism of metalation showing all intermediate species has been hard to determine, mainly because of a lack of probes that can differentiate the binding of more than one metal in dilute solutions. Recent studies have shown that mass spectrometry is able to discriminate between different intermediates and further, quantify the relative concentrations of all species present[31−35] for kinetic experiments.[36]

Shaw and Petering have reported that Cd^{2+} and Zn^{2+} metalation is largely complete at pH 7 and room temperature within the 4 ms dead-time of the stopped-flow UV−visible spectometer used.[37] On the other hand arsenic−metalation of MT occurs on a time-scale of minutes and is observable by mass spectrometry[1] making it an ideal reaction to study to obtain a detailed understanding of the metal-induced folding reactions of metallothionein. We report the first detailed As^{3+}-metalation study on the two-domain $\beta\alpha$ human metallothionein showing all intermediate As-species with correlations to the native individual single domain fragments. The data analysis reported here provides insight into the evolution of the two-domain structure because for the first time we report a property of MT that directly relates to the presence of the two domains. We report the rate constant for the first As^{3+} bound is 65% faster for the two-domain protein than for the single domain fragments and that there is an almost linear correlation between the binding rates for the incoming metal and the number of available sites. Hence, a two-domain protein binds metals dramatically faster than the individual domains. Assuming a constant k_{off}, we can for the first time, contrast that the $k_{1\beta\alpha}$ (for the first metal bound) is 6.8× greater than $k_{6\beta\alpha}$ (for the last metal bound).

Experimental Methods

Materials and Methods. Experimental procedures have previously been published; please refer to Ngu et al.[1] for further details. Recombinant human metallothionein (hMT) was expressed in BL21(DE3) *Escherichia coli* cells that were transformed using a pP-1 plasmid which contains an N-terminal S-tag (MKETAAAKFE RQHMDSPDLG TLVPRGS) as previously described.[38,39] The S-tag was removed using a Thrombin CleanCleave Kit (Sigma). The αhMT, βhMT, and $\beta\alpha$hMT proteins used in this study were based on the 43-residue, 40-residue, and 74-residue sequences, respectively. The sequence for αhMT is GSMGKAAAAC CSCCPMSCAK CAQGCVCKGA SEKCSCCKKA AAA; for βhMT is GSMGKAAAAC SCATGGSCTC TGSCKCKECK CNSCKKAAAA, and for $\beta\alpha$hMT is GSMGKAAAAC SCATGGSCTC TGSCKCKECK CNSCKKAAAA CCSCCPMSCA KCAQGCVCKG ASEKCSCCKK AAAA. There are 11, 9, and 20 cysteine residues present in αhMT, βhMT and $\beta\alpha$hMT, respectively, and no disulfide bonds. The protein was further purified and demetalated by elution through a Sephadex G25 column with a 20 mM ammonium formate buffer at pH 2.7 (Fisher). Elution was monitored by UV−visible absorption spectroscopy at the characteristic metal-free (apo) MT wavelengths of 300 to 200 nm. Fractions that contained metal-free MT were collected and purity was checked using ESI-MS. Previous reports have suggested or shown the existence of apoprotein *in vivo*[24,40−48] making the study of apoprotein relevant as a starting point in exploring the metalation reactions of As^{3+}. The apo-αhMT protein concentrations were determined from the extinction coefficients of 40,000 $Lmol^{-1}cm^{-1}$ at 220 nm, the Cd_3-βhMT protein concentrations were determined from the extinction coefficient of 36,000 $Lmol^{-1}cm^{1}$ at 250 nm, and the Cd_7-$\beta\alpha$ protein concentration was determined from the extinction coefficient of 115,000 $Lmol^{-1}cm^{-1}$ at 250 nm. The protein concentration for the kinetic ESI-MS experiment using the thermostatted-mixing tee was 19.5 μM of apo-$\beta\alpha$MT and concentrations for the timed-resolved ESI-MS experiments were 18 μM for apo-$\beta\alpha$MT, 23 μM for apo-αMT and a 30 μM for apo-βMT. Oxidation is a significant problem with solutions of MT in these experiments and the apo-proteins were maintained in their reduced state by carefully deoxygenating the

(20) Cladenone, V.; Dolderer, B.; Hartmann, H.-J.; Echner, H.; Luchinat, C.; Bianco, C. D.; Mangani, S.; Weser, U. *Proc. Natl. Acad. Sci. U.S.A.* **2005**, *102*, 51–56.
(21) Munger, K.; Germann, U. A.; Lerch, K. *EMBO J.* **1985**, *4*, 2665–2668.
(22) Munger, K.; Lerch, K. *Biochemistry* **1985**, *24*, 6751–6756.
(23) Nemer, M.; Wilkinson, D. G.; Travaglini, E. C.; Sternberg, E. J.; Butt, T. R. *Proc. Natl. Acad. Sci. U.S.A.* **1985**, *82*, 4992–4994.
(24) Krezel, A.; Maret, W. *J. Biol. Inorg. Chem.* **2008**, *13*, 401–409.
(25) Rigby Duncan, K. E.; Stillman, M. J. *FEBS J.* **2007**, *274*, 2253–2261.
(26) Chan, J.; Huang, Z.; Watt, I.; Kille, P.; Stillman, M. J. *Can. J. Chem.* **2007**, *85*, 898–912.
(27) Shaw, C. F.; He, L.; Munoz, A.; Savas, M. M.; Chi, S.; Fink, C. L.; Gan, T.; Petering, D. H. *J. Biol. Inorg. Chem.* **1997**, *2*, 65–73.
(28) Palumaa, P.; Eriste, K.; Kruusel, K.; Kangur, L.; Joernvall, H.; Sillard, R. *Cell. Mol. Biol.* **2003**, *49*, 763–768.
(29) Salgado, M. T.; Bacher, K. L.; Stillman, M. J. *J. Biol. Inorg. Chem.* **2007**, *12*, 294–312.
(30) Nettesheim, D. G.; Engeseth, H. R.; Otvos, J. D. *Biochemistry* **1985**, *24*, 6744–6751.
(31) Hathout, Y.; Fabris, D.; Fenselau, C. *Int. J. Mass Spectrom.* **2001**, *204*, 1–6.
(32) Yu, X.; Wojciechowski, M.; Fenselau, C. *Anal. Chem.* **1993**, *65*, 1355–1359.
(33) Zaia, J.; Fabris, D.; Wei, D.; Karpel, R. L.; Fenselau, C. *Protein Sci.* **1998**, *7*, 2398–2404.
(34) Daneshfar, R.; Kitova, E. N.; Klassen, J. S. *J. Am. Chem. Soc.* **2004**, *126*, 4786–4784.
(35) Shoemaker, G. K.; Kitova, E. N.; Palcic, M. M.; Klassen, J. S. *J. Am. Chem. Soc.* **2007**, *129*, 8674–8675.
(36) Wang, W.; Kitova, E. N.; Klassen, J. S. *Anal. Chem.* **2003**, *75*, 4945–4955.
(37) Ejnik, J.; Robinson, J.; Zhu, J.; Forsterling, H.; Shaw, C. F.; Petering, D. H. *J. Inorg. Biochem.* **2002**, *88*, 144–152.
(38) Merrifield, M. E.; Huang, Z.; Kille, P.; Stillman, M. J. *J. Inorg. Biochem.* **2002**, *88*, 153–172.
(39) Chan, J.; Huang, Z.; Merrifield, M. E.; Salgado, M. T.; Stillman, M. J. *Coord. Chem. Rev.* **2002**, *233−234*, 319–339.
(40) Krezel, A.; Maret, W. *Biochem. J.* **2007**, *402*, 551–558.
(41) Pattanaik, A.; Shaw, C. F. I.; Petering, D. H.; Garvey, J. S.; Kraker, A. J. *J. Inorg. Biochem.* **1994**, *54*, 91–105.
(42) Rigby, K. E.; Chan, J.; Mackie, J.; Stillman, M. J. *Proteins: Struct., Funct., Bioinf.* **2006**, *62*, 159–172.
(43) Rigby, K. E.; Stillman, M. J. *Biochem. Biophys. Res. Commun.* **2004**, *325*, 1271–1278.
(44) Hase, H.; Maret, W. *Anal. Biochem.* **2004**, *333*, 19–26.
(45) Yang, Y.; Maret, W.; Vallee, B. L. *Proc. Natl. Acad. Sci. U.S.A.* **2001**, *98*, 5556–5559.
(46) Shapiro, S. G.; Squibb, K. S.; Markowitz, L. A.; Cousins, R. J. *Biochem. J.* **1978**, *175*, 833–840.
(47) Krezoski, S. K.; Villalobos, J.; Shaw, C. F. I.; Petering, D. H. *Biochem. J.* **1998**, *255*, 483–491.
(48) Petering, D. H.; Zhu, J.; Krezoski, S. K.; Meeusen, J.; Kiekenbush, C.; Krull, S.; Specher, T.; Dughish, M. *Exp. Biol. Med.* **2006**, *231*, 1528–1534.

samples using evacuation and then saturation with argon gas such that the proteins were contained within a sealed, inert environment. All protein samples were buffered in 20 mM ammonium formate at pH 2.7.

***Caution*:** *Arsenic is a highly toxic reagent. Caution should be used when handling arsenic and its derivatives*. Solutions of 5 mM As^{3+} at pH 3.5 were prepared by dissolving As_2O_3 (AnalaR) in concentrated HCl (Caledon) and diluting with ultra pure deionized water (Barnstead). Aliquots of 7.4 M NH_4OH (Fisher) were used to raise the pH of the As^{3+} solutions. As^{3+} solutions were deoxygenated and contained within a sealed inert environment. Reactions were carried out at a pH range of 3−4 as this was the optimum range for product formation and stabilization; this pH was also suggested by Rey et al.[49] and Serves et al.[50] in order to stabilize the As^{3+}. We should mention that the structure of apo-MT in the pH range of 3−4 may have a structure different from that observed at neutral pH, which will require further study. It has been shown that MT is located in the acidic lysosomes of kidneys[51,52] and MT immunostaining in earthworms indicates that Cd-MT is located in acidic subcellular structures similar to lysosome,[53] making the study of As^{3+} binding at low pH of interest. High salt concentrations could not be used in conjunction with the ESI−MS measurements.

ESI−MS Procedures. All data were collected using a Micromass LCT mass spectrometer in the positive ion mode. The mass spectrometer was operated using the parameters: 3000.0 V capillary, 42.0 V sample cone, 4.0 V extraction cone, acquisition scan time of 4 s, and interscan delay time of 0.1 s. The ESI−MS data were processed and deconvoluted using the MaxEnt I software (Micromass). ESI−MS measurements were obtained using a wide scan range (700−2000 *m*/*z*) and MS mass calculations were integrated from a minimum of 10 scans.

Time-Resolved ESI−MS Measurements. Kinetic data were obtained by adding 10×, 15×, and 11× excess As^{3+} to solutions of apo-αhMT, apo-βhMT, and apo-βαhMT, respectively. The reaction was monitored by ESI−MS for up to110 min at 25 ± 1 °C.

Temperature-Resolved ESI-MS Measurements. Kinetic data were obtained using a thermostatted mixing "tee" attached directly to the input capillary of the ESI-MS instrument via a reaction capillary.[1] The reaction mixing time was dependent on the length, diameter and flow rate within the reaction capillary[54,55] and the short length of the input capillary. The exchangeable reaction capillary used had an inner diameter of 75 μm, with lengths ranging from 30 to 148 cm, and together with the input capillary gave reaction times of 99 to 498 s, all of which was contained within a temperature-controlled water bath. The input capillary did affect the average temperature of the reaction, particularly at the extreme high or low temperatures and short reaction times, leading to those data sets including slightly greater uncertainties. The temperature range used was 273 to 344 K. Kinetic data were obtained by mixing the two streams of solutions as shown in Figure 1 with a flow rate of 2 μL/min for the 2.5 mM As^{3+} solutions and 8 μL/min for the protein solutions, for a total flow rate of 10 μL/min, which results in a final concentration after mixing of 15.6 μM for βαhMT and a ratio for As^{3+}:βαhMT of 32:1. The temperatures reported are an average with uncertainties of ±1 K.

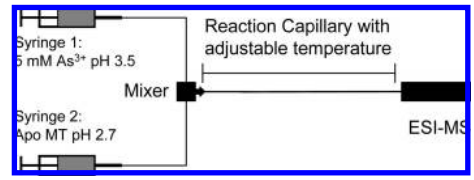

Figure 1. Schematic diagram of the continuous flow mixing set up for temperature-resolved ESI−MS measurements. Refer to the text for details.

Data Analysis. We will briefly describe the rationale behind the data analysis used in this study; further information can be found in Ngu et al.[1] The reactions shown in Figures 2, S2 and S3, all proceed to completion with the formation of As_6-H_2-βαhMT, As_3-H_2-αhMT or As_3-βhMT, respectively, with excess As^{3+} added. Under the nonequilibrium conditions of excess As^{3+} (greater than 10X excess) and the short reaction times used for the kinetic measurements reported in Figures 2−6, the reverse reactions are not significant. A series of sequential second order reactions, Scheme 1, are proposed to account for the observed kinetic data in Figures 3, 6, and 7. Scheme 1C shows the proposed order of As^{3+} binding to the domains in βαhMT. Data analysis was carried out by modeling a second order, bimolecular, irreversible mechanism with the program Gepasi.[56−58] The kinetic data for βαhMT were fitted using the six sequential bimolecular reactions of this scheme. This approach will be discussed in greater detail below. It is clear from inspection of the modeled data compared with the experimental data that the second order mechanism proposed for each step of the sequential metalation, Scheme 1, fits the experimental data exceptionally well (vide infra), Figure 3.

The measured charge state data or the deconvoluted mass spectral data were used for the kinetic analyses. Yu et al. have shown that relative concentration of various Cd-MT species can be estimated from the relative abundances of the ions in the ESI spectrum,[32] and this approach was previously shown to be reliable for analysis of kinetic data of the isolated domains.[1] The relative abundances of all the MT species observed in each mass spectrum were summed and normalized. In the time-resolved experiments, the relative abundances were plotted against time and fitted to calculate the k_n (n = 1–6 for each step in the complete metalation reaction). In the temperature-resolved experiments, the normalized relative abundances in each spectrum, following a specific reaction mixing time, were then plotted versus $1/T$ (K^{-1}), with T ranging from 273 to 344 K for each solution. As kinetic data are more readily analyzed from concentration data as a function of time at a constant temperature, our kinetic data were rearranged into this format. This serves two purposes: first, the analysis follows traditional procedures and second, the data may be directly compared to kinetic data obtained as a function of time at a fixed temperature. In addition, the data used in the subsequent analyses are averages of many different and independent data sets, which greatly improves the confidence in the calculated results. The data sets were combined in terms of ln(Relative Abundance) and appropriate interpolation points were calculated for construction of 3-dimensional graphs with the axes ln(Relative Abundance) (y-axis), time (s) (z-axis) and $1/T$ (K^{-1})(x-axis). These 3D plots are shown below in Figure 4. From these 3D plots, slices were obtained of relative abundance as a function of time at fixed temperatures. These data sets were fitted according to Scheme 1 to determine the specific temperature-dependent rate constants. Finally, the reliability of the method was confirmed by back-calculating the relative abundances of all species as a function of reaction time and temperature for comparison directly with the measured data, Figures 5 and 6.

Molecular Models. MM3/MD calculations were carried out using CAChe Workstation Pro (6.1.1) Software (Fujitsu America)

(49) Rey, N. A.; Howarth, O. W.; Pereira-Maia, E. C. *J. Inorg. Biochem.* **2004**, *98*, 1151–1159.
(50) Serves, S. V.; Charalambidis, Y. C.; Sotiropoulos, D. N.; Ioannou, P. V. *Phoshorus, Sulfur Silicon Relat. Elem.* **1995**, *105*, 109–116.
(51) Klein, D.; Lichtmannegger, J.; Heinzmann, U.; Muller-Hocker, J.; Michaelsen, S.; Summer, K. H. *Eur. J. Clin. Invest.* **1998**, *28*, 302–310.
(52) Freedman, J. H.; Powers, L.; Peisach, J. *Biochemistry* **1986**, *25*, 2342–2349.
(53) Morgan, A. J.; Sturzenbaum, S. R.; Winters, C.; Grime, G. W.; Aziz, N. A. A.; Kille, P. *Ecotoxicol. Environ. Saf.* **2004**, *57*, 11–19.
(54) Attwood, P. V.; Geeves, M. A. *Anal. Biochem.* **2004**, *334*, 382–389.
(55) Wilson, D. J.; Konermann, L. *Anal. Chem.* **2004**, *76*, 2537–2543.
(56) Mendes, P. *Comput. Applic. Biosci.* **1993**, *9*, 563–571.
(57) Mendes, P. *Trends Biochem. Sci.* **1997**, *22*, 361–363.
(58) Mendes, P.; Kell, D. B. *Bioinformatics* **1998**, *14*, 869–883.

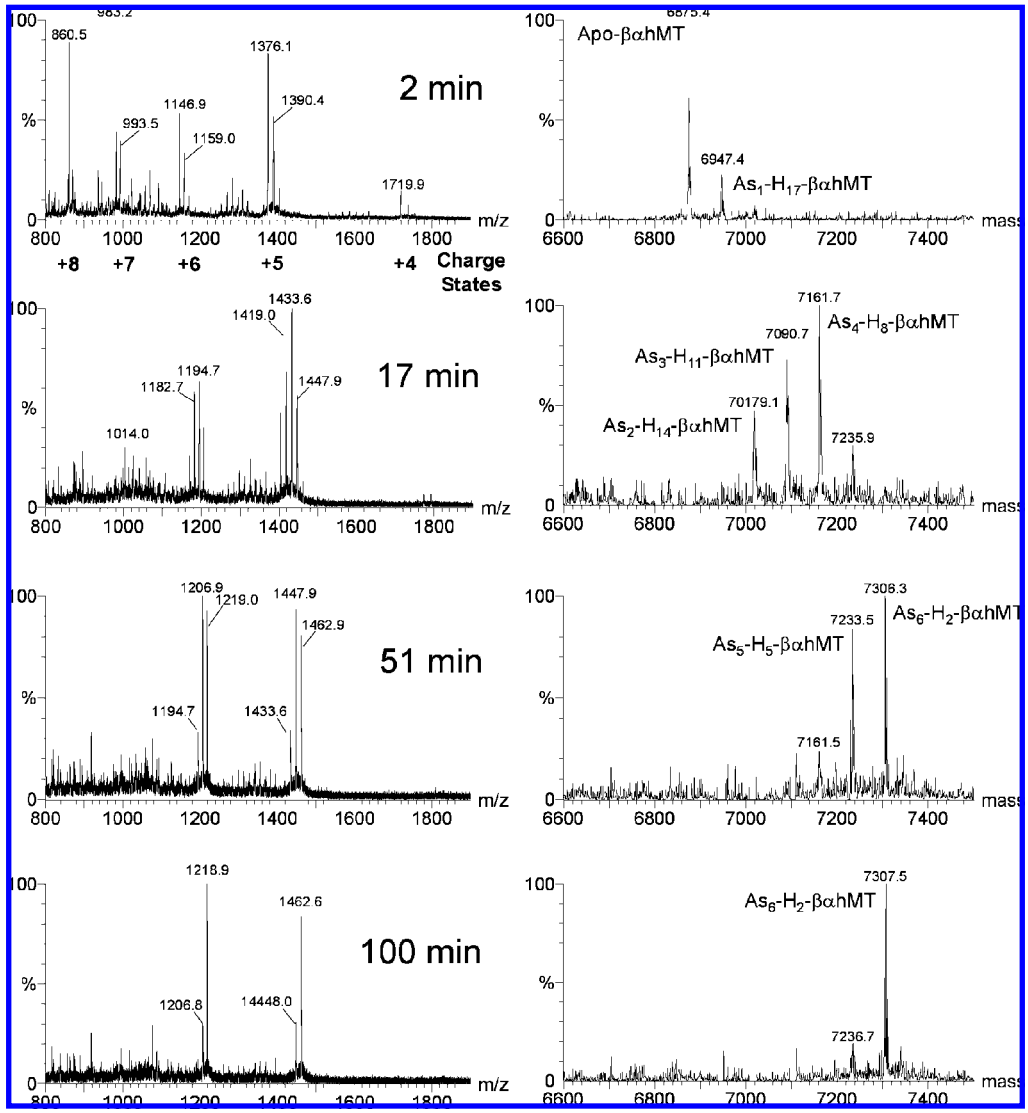

Figure 2. Time dependence of the ESI mass spectra of 18 μM apo-βαhMT in the presence As^{3+} in a stoichiometric ratio of 11:1 for As^{3+}: βαhMT. The sample was continuously monitored using ESI−MS for over 100 min at 296 K and pH 3.5.

and parametrized using the modified force field described by Chan et al.[26,59] with the dielectric constant of 80 for water to obtain energy minimized structures of the apo- and As-bound βhMT, αhMT and βαhMT proteins. An average bond length for an As-SR (R = any carbon atom) bond of 2.196 Å and an average RS-As-SR bond angle of 107.91° were used for the modeling calculation and which are consistent with As-SR crystal structures for bond length and bond angle.[60] The original apo MT structures were obtained from Chan et al.[26] and a cycle of MM3 minimizations followed by MD calculations gave the energy-minimized apo MT structures reported here. Sequential addition of As^{3+} provided the As^{3+}-bound structures as follows: the structures were first energy-minimized using the MM3 calculation followed by an MD simulation at 50 K for 100 ps and then another two MD simulations at 300 K for 1000 ps. Arsenic atoms were modeled using an sp^3 coordination and were bound sequentially as shown in Scheme 1. For βhMT the As atoms were bound sequentially along the residue sequence starting with the first 3 Cys residues on the N-terminal which would be the terminal most unlikely to be hindered in the βαhMT protein. For αhMT and βαhMT, the As atoms were bound sequentially along the residue sequence starting with the first 3 Cys residues on the C-terminal which for αhMT would be the terminal most unlikely to be hindered in the βαhMT protein and for βαhMT was the most reasonable based on the data presented later.

Results

Figures 2, S1, and S2 (Supporting Information) show the time-resolved ESI−MS spectra (with the charge states stated below the topmost spectra) measured between 2 min and up to 100 min for the As^{3+}-metalation of apo-βαhMT, apo-βhMT and apo-αhMT. Analyses of the ESI-MS data shown in Figures 2, S1, and S2 (Supporting Information) show a maximum of three As^{3+} bound to each isolated domain and six As^{3+} bound to the βαhMT protein, which corresponds to previous reports.[1,61,62] Most proteins, including metallothionein, exhibit a range of charge states due to the presence of a range of multiply charged ions. The number of charges is dependent on the number of

(59) Chan, J.; Merrifield, M. E.; Soldatov, A. V.; Stillman, M. J. *Inorg. Chem.* **2005**, *44*, 4923–4933.
(60) Iyer, R. G.; Kanatzidis, M. G. *Inorg. Chem.* **2004**, *43*, 3656–3662.
(61) Jiang, G.; Gong, Z.; Li, X.-F.; Cullen, W. R.; Le, X. C. *Chem. Res. Toxicol.* **2003**, *16*, 873–880.
(62) Toyama, M.; Yamashita, M.; Hirayama, N.; Murooka, Y. *J. Biochem. (Tokyo)* **2002**, *132*, 217–221.

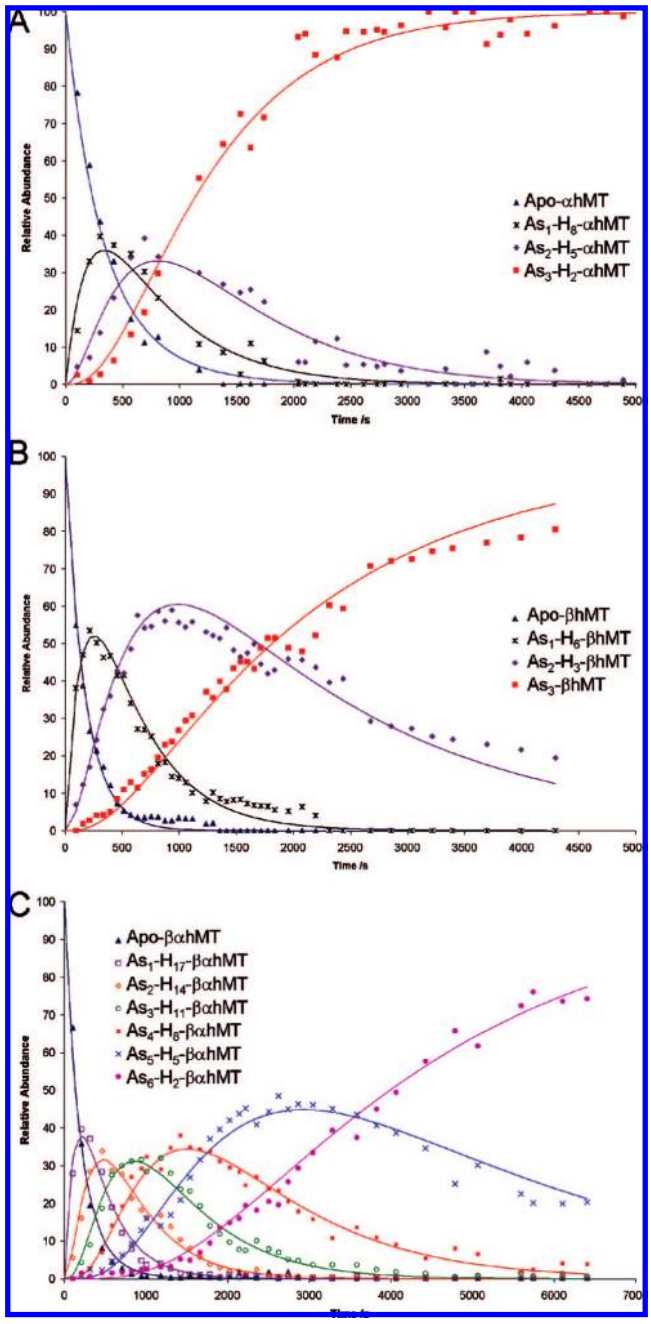

Figure 3. Time-resolved ESI-MS relative abundances for apo-αMT (A), apo-βMT (B), and apo-βαMT (C) following reaction with As^{3+} at 25 °C and pH 3.5 to form As_n-MT ($n = 1-3$ for the fragments and $n = 1-6$ for βαhMT). Reaction was carried out with an As^{3+}:MT stoichiometric ratio of 10:1 for the αhMT, a ratio of 15:1 for the βhMT, and a ratio of 11:1 for the βαhMT. Solutions of 23 μM apo-αhMT, 30 μM apo-βhMT, 18 μM apo-βαhMT and a 5 mM As^{3+} solution were used. The relative abundances for each species (apo-αhMT, apo-βhMT, and apo-βαhMT) are shown as data points on the graphs with different symbols indicating each component species. The smooth lines are calculated based on the complete analysis of the kinetic data for the relative abundance at the specified times. In each of (A), (B), and (C), the lines are connected by the series of sequential reactions shown in Scheme 1 and described in the text.

Scheme 1. Sequential Binding Mechanism Proposed for As^{3+} Binding to the (A) αhMT, (B) βhMT, and (C) βαhMT Proteins[a]

Scheme A – α MT

$$\text{Apo } \alpha\text{hMT} + As^{3+} \xrightarrow{k_{1\alpha}} As_1\text{-}H_8\text{-}\alpha\text{hMT}$$
$$As_1\text{-}H_8\text{-}\alpha\text{hMT} + As^{3+} \xrightarrow{k_{2\alpha}} As_2\text{-}H_5\text{-}\alpha\text{hMT}$$
$$As_2\text{-}H_5\text{-}\alpha\text{hMT} + As^{3+} \xrightarrow{k_{3\alpha}} As_3\text{-}H_2\text{-}\alpha\text{hMT}$$

Scheme B – β MT

$$\text{Apo } \beta\text{hMT} + As^{3+} \xrightarrow{k_{1\beta}} As_1\text{-}H_6\text{-}\beta\text{hMT}$$
$$As_1\text{-}H_6\text{-}\beta\text{hMT} + As^{3+} \xrightarrow{k_{2\beta}} As_2\text{-}H_3\text{-}\beta\text{hMT}$$
$$As_2\text{-}H_3\text{-}\beta\text{hMT} + As^{3+} \xrightarrow{k_{3\beta}} As_3\text{-}\beta\text{hMT}$$

Scheme C – βα MT

$$\text{Apo } \beta\alpha\text{hMT} + As^{3+} \xrightarrow{k_{1\beta\alpha}} H_9\text{-}\beta,\ As_1\text{-}H_8\text{-}\alpha\text{hMT}$$
$$H_9\text{-}\beta,\ As_1\text{-}H_8\text{-}\alpha\text{hMT} + As^{3+} \xrightarrow{k_{2\beta\alpha}} H_9\text{-}\beta,\ As_2\text{-}H_5\text{-}\alpha\text{hMT}$$
$$H_9\text{-}\beta,\ As_2\text{-}H_5\text{-}\alpha\text{hMT} + As^{3+} \xrightarrow{k_{3\beta\alpha}} H_9\text{-}\beta,\ As_3\text{-}H_2\text{-}\alpha\text{hMT}$$
$$H_9\text{-}\beta,\ As_3\text{-}H_2\text{-}\alpha\text{hMT} + As^{3+} \xrightarrow{k_{4\beta\alpha}} As_1\text{-}H_6\text{-}\beta,\ As_3\text{-}H_2\text{-}\alpha\text{hMT}$$
$$As_1\text{-}H_6\text{-}\beta,\ As_3\text{-}H_2\text{-}\alpha\text{hMT} + As^{3+} \xrightarrow{k_{5\beta\alpha}} As_2\text{-}H_3\text{-}\beta,\ As_3\text{-}H_2\text{-}\alpha\text{hMT}$$
$$As_2\text{-}H_3\text{-}\beta,\ As_3\text{-}H_2\text{-}\alpha\text{hMT} + As^{3+} \xrightarrow{k_{6\beta\alpha}} As_3\text{-}\beta,\ As_3\text{-}H_2\text{-}\alpha\text{hMT}$$

[a] The rate constants for each step are indicated by $k_{1-3\ (\alpha\text{ or }\beta)}$ or $k_{1-6\ (\beta\alpha)}$ which are defined as the rate of adding a single As^{3+} to the metallothionein proteins to form a product with n (1−6) As^{3+} bound. This same nomenclature is used in Table 1 where the experimental values are reported. The kinetic data were fitted for βαhMT (C) as six sequential bimolecular reactions without consideration of which domain was binding the As^{3+}.

protonatable sites, the conformation of the protein, and the pH of the solution.[1] Figures S1 and S2 (Supporting Information) show charge states of +3 and +4 for apo-βhMT, and +3, +4, and +5 for apo-αhMT. Following As^{3+}-metalation there is a dramatic shift to a nearly exclusive charge state of +4 for both species. This change in dominant charge state reflects a change in conformation of the protein[26,63,64] and suggests that the two protein fragments have rearranged into a less solvent-accessible conformation.[65] Figure 2 shows that apo-βαhMT has a charge state distribution of +4 to +8 with two dominant charge state maxima, at +5 and +7, suggesting two conformations exist in solution. Upon As^{3+}-metalation, the appearance of a dominant charge state of +5 for As_{1-4}-βαhMT suggests a more closed, solvent-inaccessible structure. Further As-metalation results in a charge state shift to +6 for As_{5-6}-βα-hMT which is consistent with the trend observed in Cd^{2+} metalation of βαhMT.[66]

The deconvoluted measured masses correlate with the theoretical masses based on the sequence shown in the Experimental Methods above. The estimated masses based on the metal content and amino acid sequence for H_{11}-αhMT, As_1-H_8-αhMT, As_2-H_5-αhMT, and As_3-H_2-αhMT are 4083.0, 4154.9, 4226.8, and 4298.8 Da, respectively, and the estimated masses based on the metal content and amino acid sequence for H_9-βhMT, As_1-H_6-βhMT, As_2-H_3-βhMT, and As_3-βhMT are 3753.5, 3825.4, 3897.3, and 3969.2 Da, respectively, and last the estimated masses based on the metal content and amino acid

(63) Dobo, A.; Kaltashov, I. A. *Anal. Chem.* **2001**, *73*, 4763–4773.
(64) Griffey, R. H.; Sannes-Lowery, K. A.; Drader, J. J.; Mohan, V.; Swayze, E. E.; Hofstadler, S. A. *J. Am. Chem. Soc.* **2000**, *122*, 9933–9938.
(65) Fenn, J. B. *J. Am. Soc. Mass Spectrom.* **1993**, *4*, 524–535.
(66) Sutherland, D. E. K.; Stillman, M. J. *Biochem. Biophys. Res. Commun.* **2008**, *372*, 840–844.

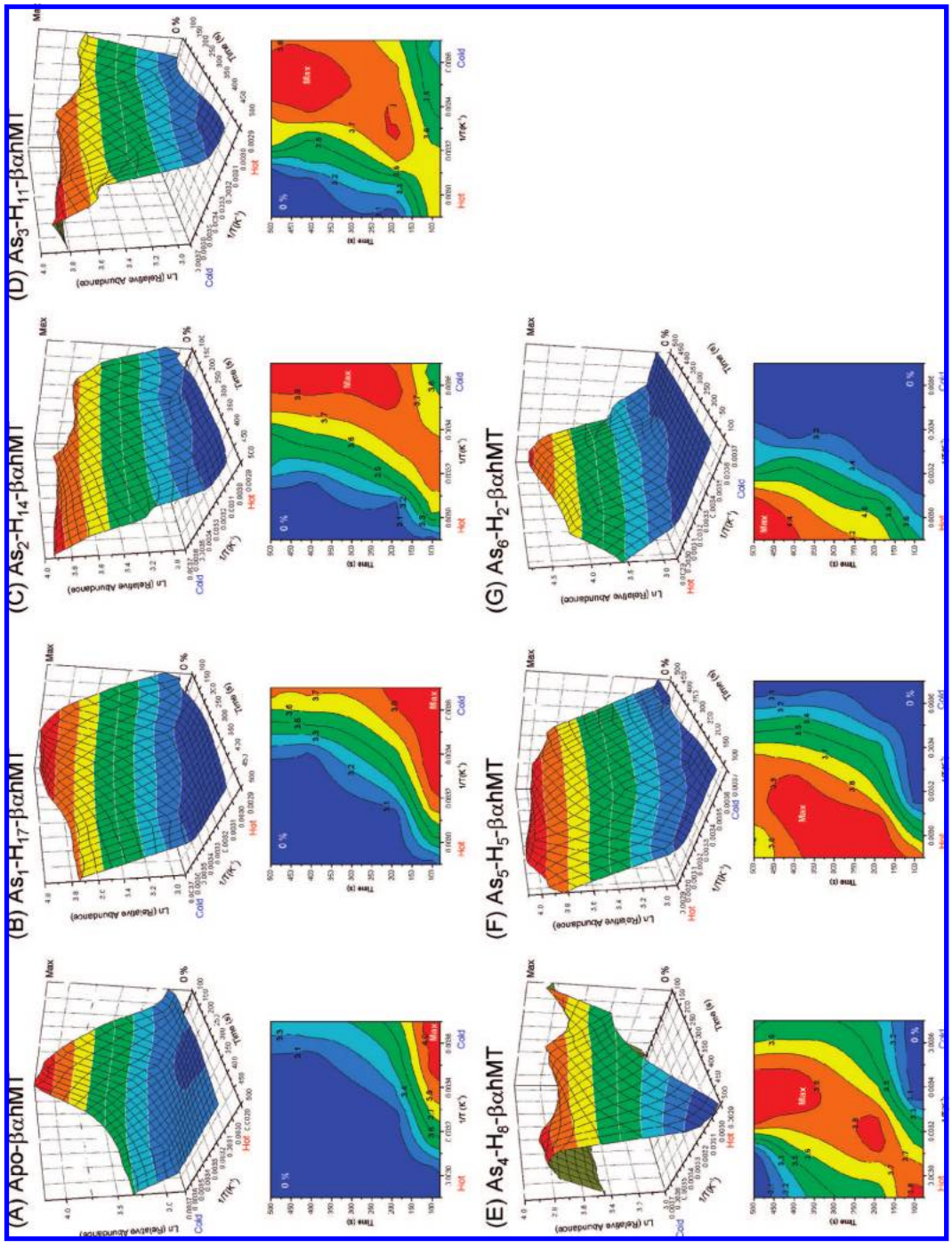

Figure 4. Trend in concentration of As_n-$\beta\alpha$hMT ($n = 0-6$) as a function of temperature, $1/T$ (K^{-1}) and time (s) following mixing with As^{3+}. The diagrams were constructed from a series of ESI−MS traces recorded between 273 and 344 K, and for reaction times between 99 and 498 s, from different solutions each with an As^{3+}:$\beta\alpha$MT stoichiometric ratio of 32:1. Solutions containing 15.6 μM apo-$\beta\alpha$MT and 0.5 mM As^{3+} were used for the measurements. (Top) 3D visualization of ln(Relative Abundance) versus $1/T$, with reaction time (s) on the *z*-axis of the single component species from the total reaction. (Bottom) Contour diagrams calculated from the 3D plots. It is important to note that to aid visualization and clarity of the trend in concentration as a function of time and temperature, each 3D plot has been orientated so that the 0% relative abundance of the specific species is at the front. For example, for apo-$\beta\alpha$hMT (A) and As_{1-4}-$\beta\alpha$hMT (B−E), the conditions for 0% relative abundances are high temperatures and long reaction times and the 3D plots are orientated such that high temperatures and long reaction times are at the front. The contour diagrams provide more detail of the reaction profiles.

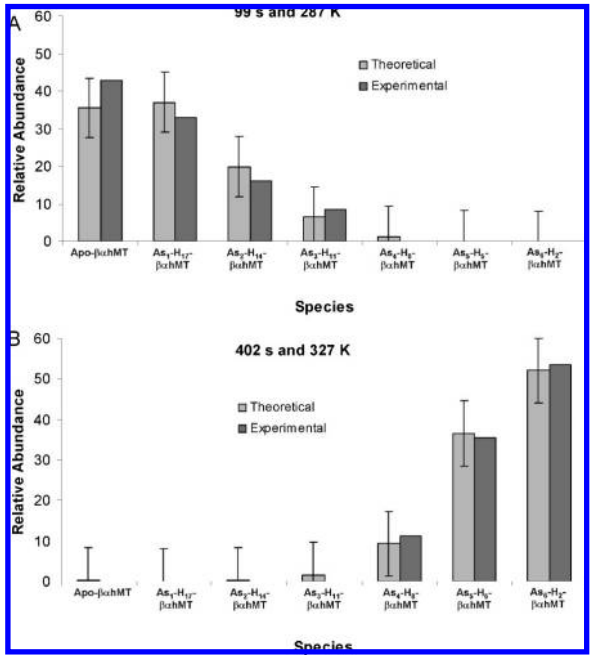

Figure 5. Comparison of experimental and theoretical relative abundances calculated for $\beta\alpha$hMT at 99 s, 287 K (A) and 402 s, 323 K (B) based on values from Table 1 and using the model shown in Scheme 1 to provide the predicted relative abundances. Conditions used were an As^{3+}: $\beta\alpha$hMT stoichiometric ratio of 32:1. Solutions containing 15.6 μM apo-$\beta\alpha$hMT and 0.5 mM As^{3+} were used for the measurements. The theoretical values from the simulation are within 10% of the experimental values. The experimental values are subject to an estimated 10% error.

sequence for H_{20}-$\beta\alpha$ hMT, As_1-H_{17}-$\beta\alpha$hMT, As_2-H_{14}-$\beta\alpha$hMT, As_3-H_{11}-$\beta\alpha$hMT, As_4-H_8-$\beta\alpha$hMT, As_5-H_5-$\beta\alpha$hMT, and As_6-H_2-$\beta\alpha$hMT are 6874.4, 6946.3, 7018.2, 7090.1, 7162.0, 7233.9, and 7305.9 Da, respectively. The masses calculated for $\beta\alpha$hMT are based on a truncated sequence resulting from the loss of the N-terminal G residue and the C-terminal AA residues without any loss of cysteine residues or change in the metal-binding capabilities of the protein. The ESI−MS measured masses closely match the theoretical masses for these species. The mass difference between the peaks in the same charge state is approximately equal to the mass of one As atom minus three protons, once again indicating that each As^{3+} binds three thiolates and displaces three protons.[1]

Figure 3 shows the As^{3+}-metalation of apo-αhMT (A), apo-βhMT (B) and apo-$\beta\alpha$hMT (C) in terms of the time-dependence of the relative abundances for the apo- and As^{3+}-bound species in the ESI-mass spectra at 25 °C. The relative abundance data points shown were obtained following normalization of the data for all species present at any single time. The experimental data were fitted (Figure 3 smooth lines) using Scheme 1 with the calculated rate constants reported in Table 1. The reaction is complete for the individual domains before 5000 s, while the 2-domain protein saturates with As^{3+} after 6000 s. The reaction of the two-domain apo-$\beta\alpha$hMT with excess As^{3+} was fitted using six sequential bimolecular reactions without consideration as to which domain the As^{3+} was binding to. The identity of the binding domain cannot be determined readily by ESI−MS as the technique can only define the number of arsenics bound based on the mass.

It has previously been shown by our group that the As^{3+}-metalation of metallothionein is time and temperature dependent for the βhMT and αhMT protein fragments containing the additional S-tag peptide.[1] Further, using ESI−MS and a

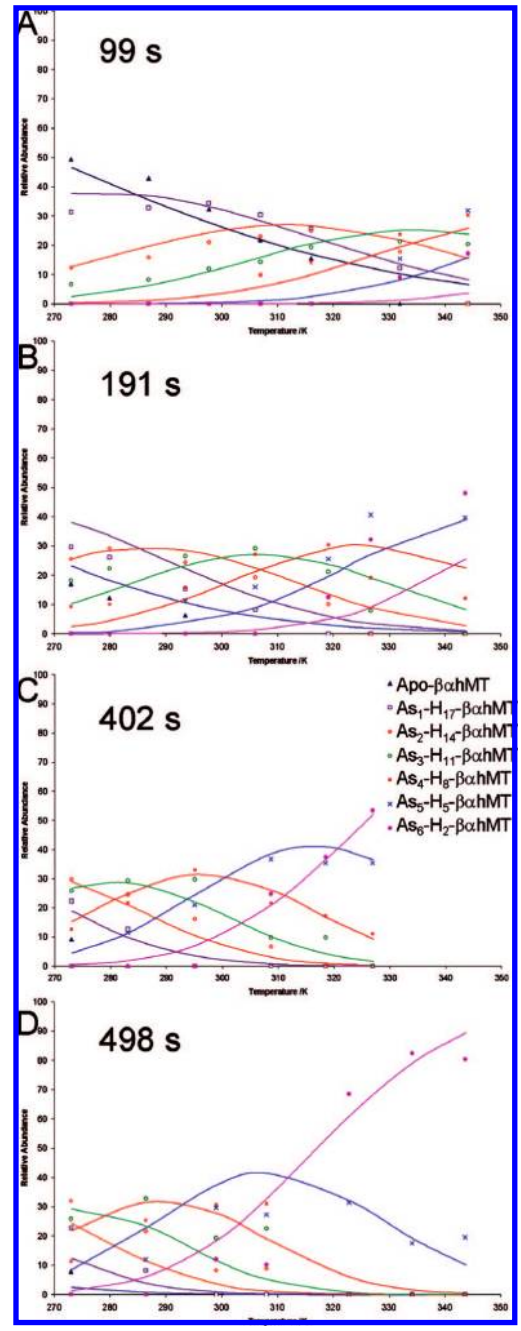

Figure 6. Temperature-resolved relative abundances of apo-$\beta\alpha$hMT and As_n-$\beta\alpha$hMT ($n = 1-6$) following reaction of apo-$\beta\alpha$hMT with As^{3+} at fixed reaction times. ESI-MS data were obtained for apo-$\beta\alpha$hMT at a series of fixed reaction times with increasing temperatures (273 − 344 K) in the presence of excess As^{3+}. The fixed reaction times were 99 s (A), 191 s (B), 402 s (C), and 498 s (D). Reaction was carried out with an As^{3+}: $\beta\alpha$hMT stoichiometric ratio of 32:1. Solutions containing 15.6 μM apo-$\beta\alpha$hMT and 0.5 mM As^{3+} were used for the measurements. The smooth lines were calculated based on the complete analysis of the kinetic data for the relative abundance of the individual component species for each temperature at the specified times. The lines are connected by a series of six sequential reactions shown in Scheme 1 and described in the text. The data points that comprise the theoretical lines were calculated from analysis of data sets measured at all reaction times and temperatures to obtain the kinetic parameters: k_{temp}, A, E_a, which were used with the experimental concentrations of the protein and the As^{3+} to predict the concentration of each species at the specified temperature and time. There will always be considerable uncertainty in any simulation that uses parameters extracted from the entire temperature-time-relative abundance data set that comprise many different experiments. The experimental values are subject to an estimated 20% error.

Table 1. Rate Constants, Activation Energies (E_A), Arrhenius Factor (A), Activation Enthalpies ($\Delta H^{\ddagger}$), Activation Entropies ($\Delta S^{\ddagger}$), and Activation Free Energies ($\Delta G^{\ddagger}$) for the As^{3+}-Induced Metalation of the $\beta\alpha$hMT

Arsenic species formed	n[a]	k_n[a] at 298 K $M^{-1}s^{-1}$	E_A[b] $kJmol^{-1}$	$A^b \times 10^4$ s^{-1}	$\Delta H^{\ddagger}$ $kJmol^{-1}$	$\Delta S^{\ddagger}$ $JK^{-1}mol^{-1}$	$\Delta G^{\ddagger}$ at 298 K $kJmol^{-1}$
As_1-H_{17}-$\beta\alpha$hMT	$1\beta\alpha$	25.2 ± 0.7	14 ± 1	0.87 ± 0.05	12 ± 1	-178 ± 37	65 ± 15
As_2-H_{14}-$\beta\alpha$hMT	$2\beta\alpha$	24.1 ± 0.8	22 ± 1	20 ± 1	16 ± 1	-164 ± 14	64 ± 7
As_3-H_{11}-$\beta\alpha$hMT	$3\beta\alpha$	19.5 ± 0.6	22 ± 1	18.0 ± 0.9	20.1 ± 0.4	-150 ± 5	65 ± 2
As_4-H_8-$\beta\alpha$hMT	$4\beta\alpha$	14.1 ± 0.3	22 ± 1	14.0 ± 0.7	25 ± 2	-138 ± 13	66 ± 8
As_5-H_5-$\beta\alpha$hMT	$5\beta\alpha$	8.7 ± 0.2	22 ± 1	8.9 ± 0.4	20 ± 2	-158 ± 19	67 ± 10
As_6-H_3-$\beta\alpha$hMT	$6\beta\alpha$	3.7 ± 0.1	22 ± 1	4.0 ± 0.2	17 ± 2	-172 ± 53	69 ± 23

[a] For reactions as shown in Scheme 1, where k_n refers to the rate constant for a single step that involves addition of a single As^{3+} forming a product with n As^{3+} bound. [b] Inspection of the lines of best fits show a clear trend for $k_{2-6\beta\alpha}$ for which these E_A are equivalent and the average is shown.

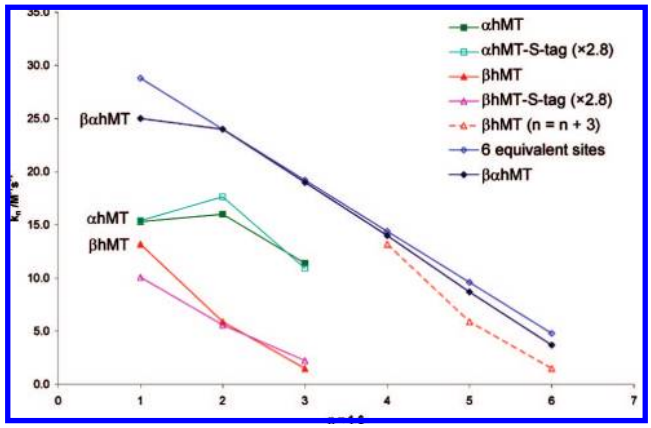

Figure 7. Comparison of the rate constants calculated from the time-resolved ESI−MS measurements for As^{3+}-metalation of αhMT, βhMT, and $\beta\alpha$hMT, the trend in rate constant values for six equivalent sites where $k_1 = 28.8\ M^{-1}s^{-1}$ and the rate constants reported for αhMT-S-tag and βhMT-S-tag.[1] The red dashed line represents rate constant data for the β hMT redrawn with the value of n shifted by three to illustrate the similarity to the rate constant trend for the final three As^{3+} binding to $\beta\alpha$hMT.

thermostatted mixing tee, it was possible to quantitatively measure the temperature-, reaction time-, and concentration-dependence of the reaction of As^{3+} with these βhMT and αhMT protein fragments.[1] In this present report, kinetic data were determined for the reaction of the more complicated, two-domain $\beta\alpha$hMT protein with excess As^{3+} for a series of fixed reaction times as a function of temperature. As described in the Experimental Methods section, the data were rearranged into a 3D representation showing the relative abundance for each of the species observed in the mass spectra: apo, As_1-, As_2-, As_3-, As_4-, As_5-, and As_6-$\beta\alpha$hMT as a function of temperature and at each reaction time. Figure 4 shows seven 3D plots, which allow for the visualization of the relative abundance of each As_n-$\beta\alpha$hMT ($n = 0-6$) species as function of temperature and reaction time. The contours included in Figure 4 also allow for each species' relative concentration to be determined as a function of temperature and reaction time. Multiple sets of data at a fixed temperature were extracted from these 3D plots and analyzed using the sequential second-order reaction mechanism shown in Scheme 1. The temperature-dependent rate constants were obtained and plotted as $\ln(k)$ versus $1/T$ (K^{-1}) (Figure S3A, Supporting Information) and as $\ln(k/T)$ versus $1/T$ (K^{-1}) (Figure S3B, Supporting Information) to evaluate activation energies, Arrhenius factors, and the Erying transition state parameters (Table 1).

The activation energies and Arrhenius factors in Table 1 were used to simulate the theoretical relative abundance of each As_n-$\beta\alpha$hMT ($n = 0-6$) for every experimental data point obtained at fixed times and varying temperatures during the temperature-resolved experiments (Figures 5 and 6). Figure 5 shows a comparison of the relative abundances of As_n-$\beta\alpha$hMT ($n = 0-6$) for two simulations (99 s at 287 K and 402 s at 327K) with the respective experimental data. In both Figure 5A and B, the predicted relative abundances in the simulation are within 8% of the experimental relative abundances. The predominant species present at 99 s and 287 K (Figure 5A) are apo- and As_1-$\beta\alpha$hMT; upon increasing the reaction times and temperature to 402 s and 327 K (Figure 5B) the predominant species shifted to the more As^{3+}-loaded species, As_5- and As_6-$\beta\alpha$hMT. This test uses fitted parameters from analysis of all the experimental data for each species, for example, 27 data sets were used to calculate the parameters.

To further test the validity of the method and the accuracy of the parameters derived in Table 1, we simulated the normalized abundance of each species for the fixed reaction times of 99, 191, 402, 498 s at increasing temperatures, for all experimental data used for the temperature-resolved experiments (Figure 6). The smooth lines in Figure 6 are simulations of the six simultaneous bimolecular reactions occurring over the range of temperatures and times shown, which are described by 27 individual data sets. The simulations are dependent on the calculated specific rate constants for the specified temperature and the activation energies and Arrhenius constant, A, shown in Table 1. Considering the inherent uncertainties of the experimental data and the extent to which each component interconnects, such that errors in the relative abundance of one species for the data set will introduce compensating errors in the relative abundance of the other species, we suggest the simulations are in remarkably good agreement with the experimental normalized concentrations. We assess the uncertainties as up to 20%.

Taking a closer look at Figure 6A shows that at 99 s and low temperatures, the dominant species present was apo-$\beta\alpha$hMT, but following heating, the apoprotein is consumed to form As_1-H_{17}-$\beta\alpha$hMT, which in turn is consumed to form further intermediates with greater As^{3+} content. Figure 6D shows that at 498 s and low temperatures, there is a mixture of As-intermediates already formed compared with the situation at 99 s, hence the reaction has proceeded further toward completion, as expected. At high temperatures and for the reaction time of 498 s, nearly all the apo-$\beta\alpha$hMT has reacted to form the final product, As_6-H_2-$\beta\alpha$hMT

Discussion

Metalloproteins are considered to represent 30% of all proteins, yet there is a lack of detailed understanding about the metalation process itself. In general, one can separate the metalation process into two categories, (i) metalation of an apoprotein that is already folded and in its native conformation, and (ii) metalation that results in significant folding of the apoprotein that may be identified as metal-induced folding. It is clear from all previous work, that in metallothioneins, metal-

induced folding is the major force controlling folding to the native state, playing a more important role than the typical interaction forces of H-bonding and hydrophobicity. In this present study, we report on the mechanism of metalation for the two-domain, human metallothionein, which is a model for metalloproteins with multiple metal-binding sites for which metal-induced folding applies.

Metallothionein is ubiquitous in Nature, highlighting its significance in the cellular chemistry of metals. As one of the most prominent multiple-metal-binding proteins in the natural world, an understanding of the mechanism for metalation of metallothioneins is needed and this mechanism will serve as an excellent model for other metalloproteins where the metal or metals dominate the formation of the secondary and tertiary structure.

Our mechanistic studies reported in this paper extend our previously reported slow metalation reaction of As^{3+} with the isolated metallothionein fragments.[1] In this paper, we report the metalation of the two-domain human metallothionein, comparing the rates of binding up to six As^{3+} into the two-domains with the rates for binding up to three As^{3+} into the two isolated fragments. Mammalian metallothionein exists only as the two-domain protein yet no conclusive explanation of the evolutionary advantage for the two-domains has been put forward. Comparisons between the metalation data of the isolated fragments and the two-domain protein have previously been difficult because the rates of metalation are typically too fast to measure even by stopped-flow techniques. In the experimental methods used in the present study, the metal binding rates are slow enough to allow complete determination of all the kinetic parameters for each metal and further, we have available the complete data for both the isolated fragments and the two-domain protein.

Mechanism of Binding for As^{3+}. A recent paper reports the potential use of seaweed MT, expressed in *Escherichia coli* cells to remediate As^{3+} in drinking water,[67] which will require an understanding of the As^{3+} metalation chemistry for the development of the remediation technology. As^{3+}-metalation of MT in the mammalian system is also important in understanding the in vivo chemistry of As^{3+} and its metabolic pathway following ingestion from seafood and drinking water. Studies by Graham[68−70] and Rosen[71] have shown that there are two potential mechanisms by which arsenic may be detoxified from the human body. Both detoxification pathways involve thiol-containing proteins and peptides binding As^{3+} and in the case of the arsenic reductases, the reduction of As^{5+} to As^{3+}.[71] Clearly, the cysteine-rich metallothioneins may play an important role in As^{3+} metabolism.

While previous mechanistic results were for the isolated single-domain fragments, the data presented here are for the complete, two-domain protein. Scheme 1 shows a mechanism for the sequential binding of six As^{3+} to both domains. Analysis of the experimental data using this model provided good fits to the experimental time- and temperature-dependent data, which we consider to support the validity of the mechanism in Scheme 1. This study confirms the binding stoichiometry of three and six As^{3+} bound to the single fragments and the two-domain MT, respectively, as reported in previous studies.[1,61,62] The presence of As^{3+}-species with fewer than these numbers of As^{3+} bound indicates noncooperative sequential binding rather then a cooperative mechanism. There was no evidence of thiolate-bridging in any of the three protein species, because if thiolate-bridging were to occur then we believe the remaining two cysteines in the 11 Cys-αhMT and 20 Cys-βαhMT would bind an additional As^{3+} ion, bringing the saturated levels to four and seven, respectively, for the fragments and two-domain protein. This also implies that there is no cluster formation as typically observed with other metals like Cd^{2+}. Based on the masses obtained from the ESI-MS data, we can determine that each As^{3+} binds to three sulfurs, displacing three protons, implying a distorted trigonal conformation based on arsenic's typical coordination chemistry with a nonbonding electron pair blocking the fourth site of the tetrahedron.[72]

Comparison and Implications of the Values of the Rate Constants. Figure 7 shows a comparison of the rate constants calculated for As^{3+}-metalation of βhMT, βhMT-S-tag, αhMT, αhMT-S-tag, and βαhMT. The βhMT-S-tag and αhMT-S-tag protein from Ngu et al.[1] contained an additional short amino acid sequence (S-tag) in the MT residue sequence, which was part of the protein expression system. It is clear, now that kinetic data for the thrombin-cleaved fragments have been obtained, that the presence of the S-tag slowed the binding rates of the protein but did not affect the overall mechanism of As^{3+} binding. MD calculations have previously shown the S-tag is quite fluxional and does not adopt a fixed or even sticky association with MT.[26] However, we believe the S-tag acts in these As^{3+}-metalation studies by periodically blocking the binding site. This blocking action slows the metalation reaction rates but our analysis shows that it does not change the mechanism of As^{3+}-metalation.

To compare the rates of metalation of the previous S-tag-containing fragments with the data reported in the study for which the S-tag had been cleaved, as shown in Figure 7, we have scaled the rate constants for the S-tag containing protein by an empirically determined factor of 2.8. The trends now displayed in Figure 7 are similar for both sets of fragment data and confirms that the rate constants in this paper are consistent with those reported earlier.[1]

Figure 7 summarizes all the trends observed in the rate constants for the two-domain protein and the individual single fragments. The significant and novel result reported here is that the two-domain protein binds the initial As^{3+} ions considerably faster than the isolated domains and that the rate constants systematically diminish as a function of the remaining sites. The trends in rate constants for each species guide our interpretation of the overall metal-binding properties of the βαhMT protein. For each fragment, the reduction in rate constants as a function of As^{3+}-bound also follows the same dependence on the number of available unoccupied binding sites. Additionally, the nonlinear behavior of the rate constants for the first As^{3+} bound to apo-αhMT and apo-βαhMT, we propose,

(67) Singh, S.; Mulchandani, A.; Chen, W. *Appl. Environ. Microbiol.* **2008**, *74*, 2924–2927.
(68) Gailer, J.; George, G. N.; Pickering, I. J.; Prince, R. C.; Ringwald, S. C.; Pemberton, J. E.; Glass, R. S.; Younis, H. S.; DeYoung, D. W.; Aposhian, H. V. *J. Am. Chem. Soc.* **2000**, *122*, 4637–4639.
(69) Gailer, J.; George, G. N.; Pickering, I. J.; Prince, R. C.; Younis, H. S.; Winzerling, J. J. *Chem. Res. Toxicol.* **2002**, *15*, 1466–1471.
(70) Manley, S. A.; George, G. N.; Pickering, I. J.; Glass, R. S.; Prenner, E. J.; Yamdagni, R.; Wu, Q.; Gailer, J. *Chem. Res. Toxicol.* **2006**, *19*, 601–607.
(71) Demel, S.; Shi, J.; Martin, P.; Rosen, B. P.; Edwards, B. F. P. *Protein Sci.* **2004**, *13*, 2330–2340.
(72) Housecroft, C. E.; Sharpe, A. G. *Inorganic Chemistry*, 2nd ed.; Pearson Prentice Hall: Harlow, England, 2005.

arises from structural properties of the metal-free protein α domain. We will now address the following key features from Figure 7:

(i) $K_{1\beta}$ Is Less for S-Tag-Containing βhMT than the S-Tag-Free Fragment. The first rate constant, $k_{1\beta}$ for the first As^{3+} bound to the βhMT-S-tag-free protein is greater than that of the adjusted $k_{1\beta}$ for the S-tag bound βhMT protein. We believe this is because the S-tag-free protein can bind the first As^{3+} ion from both the N- and C-terminals whereas the N-terminal bound S-tag containing protein can only readily bind the first As^{3+} from the C-terminal, statistically reducing the rate.

(ii) $k_{1\alpha} < k_{2\alpha}$ for αhMT. The rate constants for the first two As^{3+}-metalation steps of apo-αhMT exhibit the reverse order than expected, that is $k_{1\alpha} < k_{2\alpha}$; this was observed in the data for both this report and the previous report.[1] Duncan et al. have proposed that the apo-αhMT adopts a structure as a result of metal templating instead of existing as a simple random coil.[42,43,73] If this was the case, then the first As^{3+} to bind apo-αhMT may need to disrupt this structure, thereby allowing the succeeding As^{3+} to bind more readily and resulting in $k_{1\alpha} < k_{2\alpha}$. The data suggest the first As^{3+} binds to the C-terminal because the reduction in $k_{1\alpha}$ is similar for both the S-tag-free and S-tag containing fragments.

(iii) The Rate Constant Values for Each Successive As^{3+} Bound in βαhMT Decrease Approximately by a Factor of 1/6 per As^{3+} Bound. The six experimentally determined rate constants for the two-domain βαhMT protein are shown as function of the number of As^{3+} bound in Figure 7. With the exception of $k_{1\beta\alpha}$ the trend in the rate constant values is that predicted for the presence of six equivalent binding sites. The predicted magnitude of each k_n ($n = 1-6$) for six equivalent sites diminishes as a function of the number of unoccupied sites available for the incoming metal, that is, $k_1 = 6/5k_2 = 3/2k_3 = 2k_3 = 3k_5 = 6k_6$, where the predicted value of k_1 is 28.8 $M^{-1}s^{-1}$.

(v) The Trend in $k_{1\beta\alpha}$ Is Reminiscent of the Trend in $k_{1\alpha}$. The reduced $k_{1\beta\alpha}$ is also found for the As-metalation of apo-αhMT and apo-αhMT-S-tag (Figure 7). Our interpretation of the reduction in $k_{1\beta\alpha}$ is based on the same argument used in point (ii) in which hindered access to the binding sites for the metal-template structure slows the metal-binding process. We propose from this analysis that the majority of the first As^{3+} is bound to the C-terminus of the α domain in βαhMT based on the trend observed for $k_{1-2\beta\alpha}$. We suggest, however, that the small increase between $k_{1\beta\alpha}$ and $k_{2\beta\alpha}$, arises from a small fraction of As^{3+} binding to the N-terminal β domain in the βαhMT.

(vi) $k_{1-3\beta}$ Are Relatively Close in Value to $k_{4-6\beta\alpha}$. In Figure 7, the rate constants, $k_{1-3\beta}$ for βhMT are also shown shifted by $n = 3$ places to align them with $k_{4-6\beta\alpha}$ for βαhMT and to emphasize the relative closeness of these values to the last three rate constants for βαhMT. On the basis of this similarity in values between $k_{1-3\beta}$ and $k_{4-6\beta\alpha}$, we propose that the last three As^{3+} are bound to the β domain of βαhMT.

Implications of the Values of the Kinetic and Erying Transition State Parameters. Table 1 lists the activation energies for the reaction forming each As_n-βαhMT species ($n = 1-6$). E_A increases from 14 $kJmol^{-1}$ for H_9-β, As_1-H_8-βαhMT to 22 $kJmol^{-1}$ for the remaining As_n-βαhMT species ($n = 2-6$). For As_n-βαhMT ($n = 2-6$), the activation energies listed are an average of all the E_A's for $k_{2-6\beta\alpha}$ calculated from the lines of best fit of the Arrhenius plots. Figure S3 (Supporting Information) shows the Arrhenius plot and Erying plot for $k_{1-6\beta\alpha}$. It can be seen in Figure 3A that with the exception of the $1/T$ dependence of $k_{1\beta\alpha}$, the trend in $1/T$ dependence of k_n are very similar, hence to calculate the E_A we set the slope of the $1/T$ dependence of $k_{2-6\beta\alpha}$ to the average value for these five reactions. The data in Figure S3A (Supporting Information) show that the E_A is essentially the same for all but the first As^{3+} bound. We conclude, therefore, that the As^{3+}-metalation of apo-βαhMT is controlled by the Arrhenius factor, in other words, the statistical frequency of collisions that occur with the correct orientation and result in product formation.

The Erying Transition State Parameters $\Delta H^{\ddagger}$, $\Delta S^{\ddagger}$, and $\Delta G^{\ddagger}$ correspond to those calculated by Ngu et al.[1] and provides further evidence that the underlying chemistry for As^{3+}-binding to βαhMT is the same as that observed in the isolated, individual α and β domains.

Molecular Modeling of As-Metalated MT. Figures 8 and 9 shows molecular models constructed from the energy-minimized structures for the metal-free and the As^{3+}-loaded βhMT, αhMT and βαhMT proteins. In the absence of any As-MT X-ray crystal or NMR structures, these molecular models provide an initial visual framework to aid in our understanding of the As^{3+}-metalation mechanism and possible final structures. The apo structures of all three constructs shown in Figure 8 and 9 are somewhat globular with the sulfurs exposed to the solvent as first reported by Rigby et al.[42,43] Refering to the ESI-MS data we see that addition of the first As^{3+} ion to the αhMT or the βhMT protein resulted in a collapse of multiple charges for the metal-free proteins to a single dominant charge state (Figures S1−S2, Supporting Information). The molecular models show that a single addition of one As^{3+} atom to apo-βhMT or apo-αhMT results in formation of another globular structure but where the sulfurs are more shielded by the peptide chain. Further additions of As^{3+} to the βhMT or αhMT proteins do not change the charge state distributions observed (Figures S1 and S2, Supporting Information), which may be the result of formation of similar globular structures predicted by the molecular modeling (Figure 8).

The molecular models for βαhMT are shown in Figure 9. The MS spectra for As-metalation of apo-βαhMT (Figure 2) show apo-βαhMT has two dominant charge states (+7 and +5), which give way to the single dominant charge state of +5 when As_4-H_8-βαhMT is most abundant and then shifts to the dominant charge states of +6 and +5 for As_6-H_2-βαhMT. Similarly to the As_n-α/βhMT ($n = 1-3$) molecular models, the MD energy-minimized βαhMT structures show that the metal-free protein coalesces to a globular structure in which the two domains intermingle and the sulfurs are exposed to the solvent. Following binding of 1−4 As^{3+} atoms, the structure of the protein, though still globular, is more compact with the unbound sulfurs still exposed on the surface. The binding of the fifth and sixth As^{3+} ion results in another globular conformation where the $As-Cys_3$ units are buried inside the protein

Why Is Mammalian MT a Two-Domain Structure? The two-domain evolutionary advantage of the mammalian MT has been speculated on for a long time, particularly compared to single-domain MT. In this present study, we analyzed kinetic data for the As^{3+}-metalation of the two-domain human MT and compared these results to the isolated domain fragments. The metalation involved a noncooperative sequential binding mechanism where, we propose, the data show the α domain and then the β domain bind As^{3+} atoms sequentially along the amino acid sequence starting with the first three cysteines from the

(73) Rigby Duncan, K. E.; Stillman, M. J. *J. Inorg. Biochem.* **2006**, *100*, 2101–2107.

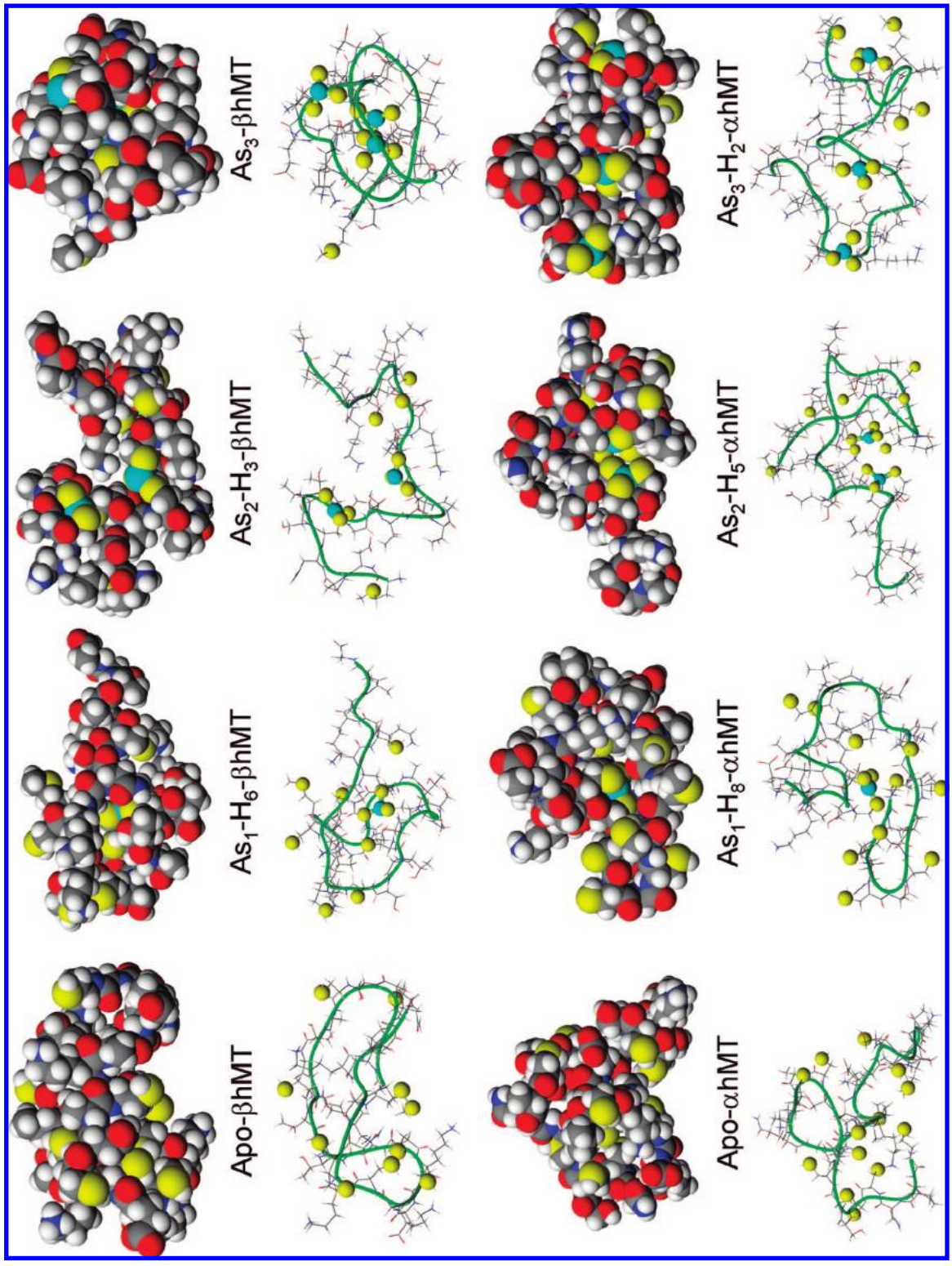

Figure 8. Ribbon and space-filling representations of energy-minimized molecular models of As_n-βhMT and As_n-αhMT ($n = 0-3$). The yellow colored atoms correspond to sulfur atoms and the teal atoms correspond to As^{3+} atoms. Each As-Cys_3 metal center has a distorted trigonal coordination.

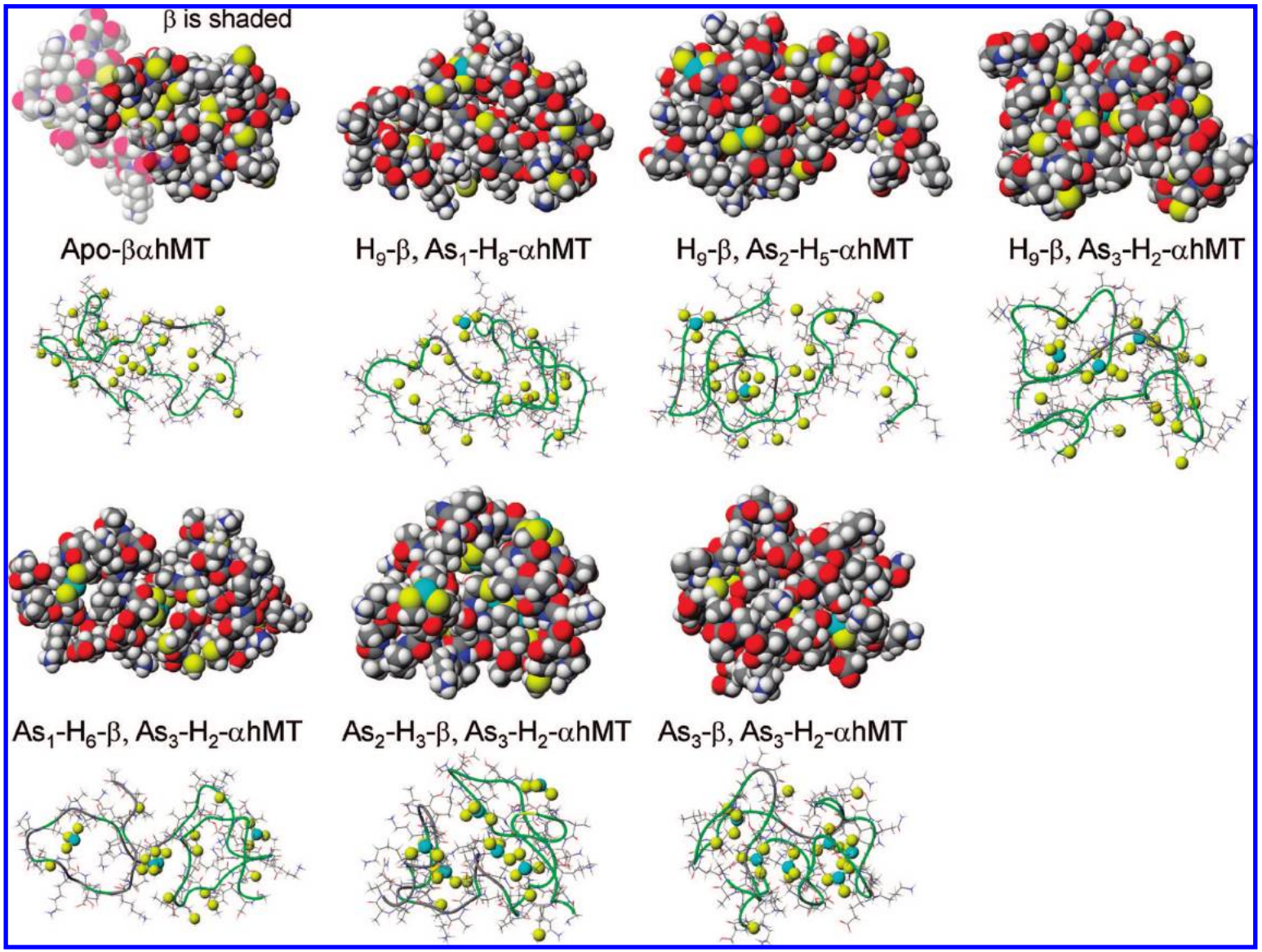

Figure 9. Ribbon and space-filling representations of energy-minimized molecular models of apo-βαhMT and As_n-βαhMT ($n = 1-6$). The β domain is shaded in the apo-βαhMT structure to emphasize its conformation relative to the α domain. The yellow colored atoms correspond to sulfur atoms and the teal atoms correspond to As^{3+} atoms. Each As-Cys_3 metal center has a distorted trigonal coordination.

C-terminal. We further showed that in βαhMT the metalation rate of the five equivalent binding sites are controlled by the statistical probability of a collision with the correct orientation occurring.

The key result we report is that the initial rate constant values for the separate single domain fragments are significantly slower than the initial rate constant of the two-domain protein for As^{3+}-metalation. This observation, we propose, is a consequence of βαhMT having six binding sites compared to the three binding sites in the individual fragments and reflects how an increase in the number of binding sites directly results in an increase in the rate constants values for the two-domain protein. For a protein, increasing the number of equivalent binding sites, therefore, increases the rate at which the protein will bind the first few metals. If the dissociation reaction occurs with the same rate for each site then this differential in binding rates results in significantly different binding constants for the first and last metal bound. For MT this implies that the change from a single-domain protein to a two-domain protein, results in the two-domain MT being able to bind metals faster and more efficiently, hence becoming a superior metal scavenger; one of MT's proposed functions.

A number of reports have been published that describe properties of MT that may be explained by our proposed explanation for metallothionein's two-domain structure. We outline one such property now. Partially metalated MT[7,24] has been reported and noncooperative binding mechanisms for Zn^{2+} and Cd^{2+} [25,66,74] have been demonstrated. On the basis of our proposal that an increase in the number of binding sites will increase the rate constant values (and the binding constants) for noncooperative binding, we can explain why partially metalated MT may exist. From a coordination chemistry point of view, with a large number of equivalent binding sites, it is quite reasonable that one or more of these sites may be unoccupied. Only in the presence of a large excess of metals will the last binding site be occupied. But it is well-known that MT induction takes place rapidly so that in the cell there will always be sufficient MT to reduce metal concentrations quite reasonably resulting in the presence of partially metalated MT.

Progress in Understanding Metalation Reactions of Metalloproteins and Metallothionein. A review by Gray in 2003 states that one of the major growth areas for inorganic biochemistry will be the study of how peptides/proteins fold around metals.[75] Even now, few metalation/folding studies of metalloproteins or peptides have been reported.[76] To the best of our knowledge there are only a small number of reports on the kinetics of metalation or demetalation reactions of metallothionein.[1,28,31,33,37,77,78] We have described here for the first time the complete kinetic analysis for the arsenic-induced metalation of the two-domain βαhMT and show the sequential rate constants for each step of the metalation reaction. These data show that human metallothionein binds arsenic sequentially rather then cooperatively and the order of domain loading appears to be α then β with respect to As^{3+}. Our results provide direct evidence for the evolution of the two-domain metallothionein protein.

Acknowledgment. We thank NSERC of Canada for financial support through operating funds (to M.J.S.) and the NSERC Canadian Graduate Scholarship (to T.T.N.). We thank Prof. R. J. Puddephatt for use of the ESI−MS funded by the Canada Research Chair program. We are grateful to Doug Hairsine for advice and discussion on the operation of the ESI−MS.

Supporting Information Available: Three figures (S1−S3) with descriptive text are provided that show timed-resolved ESI−mass spectral data, the Arrhenius plot, and the Erying plot referred to in the text. This material is available free of charge via the Internet at http://pubs.acs.org.

JA8060326

(74) Palumaa, P.; Eriste, E.; Njunkova, O.; Pokras, L.; Joernvall, H.; Sillard, R. *Biochemistry* **2002**, *41*, 6153–6158.

(75) Gray, H. B. *Proc. Natl. Acad. Sci. U.S.A.* **2003**, *100*, 3563–3568.

(76) Ghosh, D.; Pecoraro, V. L. *Inorg. Chem.* **2004**, *43*, 7902–7915.

(77) Krepkiy, D.; Antholine, W. E.; Petering, D. H. *Chem. Res. Toxicol.* **2003**, *16*, 750–756.

(78) Salgado, M. T.; Stillman, M. J. *Biochem. Biophys. Res. Commun.* **2004**, *318*, 73–80.